ACS SENSORS

Article

pubs.acs.org/acssensors

Direct, Label-Free, and Rapid Transistor-Based Immunodetection in Whole Serum

Óscar Gutiérrez-Sanz,[†] Nesha M. Andoy,[†] Marcin S. Filipiak,[†,‡] Natalie Haustein,[†,§] and Alexey Tarasov*[,†,‡]

[†]BioMed X Innovation Center, 69120 Heidelberg, Germany

[‡]Institute for Physical Chemistry, Universität Heidelberg, 69120 Heidelberg, Germany

[§]Institute for Materials Science, Technische Universität Dresden, 01062 Dresden, Germany

Supporting Information

ABSTRACT: Transistor-based biosensors fulfill many requirements posed upon transducers for future point-of-care diagnostic devices such as scalable fabrication and label-free and real-time quantification of chemical and biological species with high sensitivity. However, the short Debye screening length in physiological samples (<1 nm) has been a major drawback so far, preventing direct measurements in serum. In this work, we demonstrate how tailoring the sensing surface with short specific biological receptors and a polymer polyethylene glycol (PEG) can strongly enhance the sensor response. In addition, the sensor performance can be dramatically improved if the measurements are performed at elevated temperatures (37 °C instead of 21 °C). With this novel approach, highly sensitive and selective detection of a representative immunosensing parameter—human thyroid-stimulating hormone—is shown over a wide measuring range with subpicomolar detection limits in whole serum. To the best of our knowledge, this is the first demonstration of direct immunodetection in whole serum using transistor-based biosensors, without the need for sample pretreatment, labeling, or washing steps. The presented sensor is low-cost, can be easily integrated into portable diagnostics devices, and offers a competitive performance compared to state-of-the-art central laboratory analyzers.

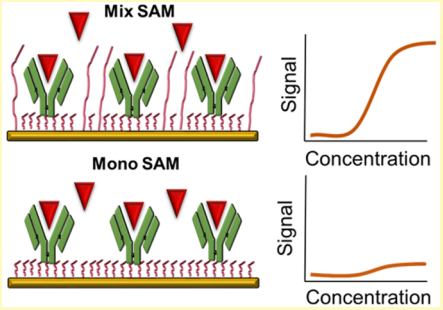

KEYWORDS: *Debye length, field-effect transistor (FET), biosensor, thyroid-stimulating hormone (TSH), label-free, serum*

Field-effect transistor (FET) based biosensors[1−3] are ideal candidates for future use in point-of-care diagnostics devices (PoC)[4] due to their advantageous characteristics compared to other biosensor types. These purely electronic devices have a fast response and can be inexpensive, miniaturized, and mass-fabricated using conventional nano- and microfabrication technology. They have demonstrated high sensitivity and selectivity in label-free detection schemes of various analytes including electrolyte ions, DNA, small molecules, proteins, and cells.[3,5−14] Despite these attractive properties not many commercial applications have appeared in the market (i.e., Ion AmpliSeq technology[15] or Vista's silicon nanowire FET based NanoBioSensor[16]) since the first FET biosensor demonstration in the late 1970s.[9,17] This is partly due to a major drawback of this technology, the so-called Debye screening in physiological solutions.[18−21]

FET-based biosensors sense the change in the electric field caused by the binding of charged target species on the sensor surface, resulting in changes in the measured channel current.[22] This basic operating principle can become ineffective if the target molecules are to be detected in high ionic strength solutions such as blood or serum, because the effective charge of the analyte is screened by the electrolyte ions. This effect is called Debye screening and the characteristic distance that defines how far this effect persists is the Debye screening length (λ_D).[23] In physiological conditions, λ_D is <1 nm, making the direct detection in real samples difficult because the size of the typical receptor molecules exceeds this length.[19,20]

To address this challenge, several interesting yet relatively complex strategies have been proposed that require additional sample pretreatment, multiple washing steps, or more advanced sensor geometry and instrumentation, limiting their applicability in a point-of-care setting.[18,20,24,25] Another promising and direct approach is the use of shorter receptors with different orientation and spacing.[24,26,27] It remains unclear, however, to what extent this can be generalized since most of the receptors are larger than the critical Debye length in physiological conditions (<1 nm). More recently, the addition of a polymer that can increase the effective Debye screening length has been proposed as a more general approach.[20,28] Unfortunately, only buffer solutions have been used to date with moderate detection limits in the 100 nM range for specific biosensing,[28] which is not suitable for many clinically relevant parameters that require picomolar detection limits in serum.

Received: March 24, 2017
Accepted: August 3, 2017
Published: August 30, 2017

DOI: 10.1021/acssensors.7b00187
ACS Sens. 2017, 2, 1278−1286

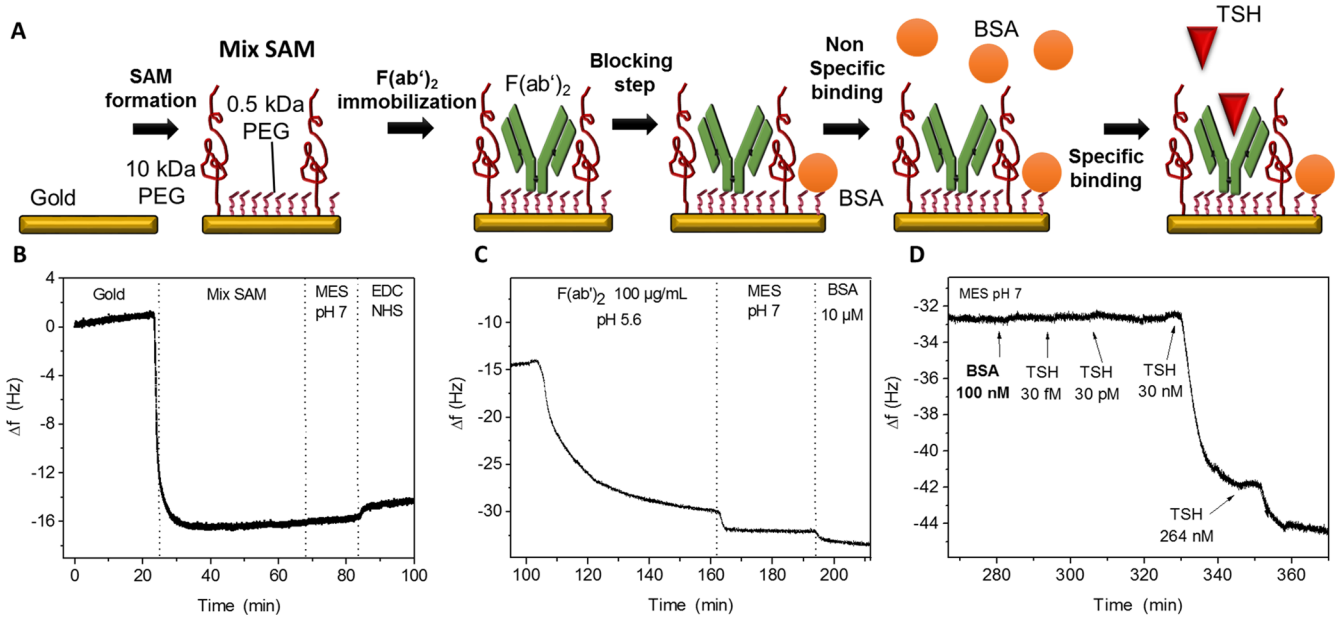

Figure 1. (A) Schematic representation of the main modification steps of the gold electrodes. (B,C,D) Quartz crystal microbalance (QCM) data of the gold modification protocol and test of TSH binding to $F(ab')_2$ fragments. (B) Frequency response of the gold-coated QCM chip to the immobilization of the Mix SAM, removal of the Mix SAM excess with MES buffer and the activation of the SAM with EDC/NHS. (C) Immobilization of $F(ab')_2$ fragments on the activated surface followed by addition of 10 μM BSA to block the active surface sites not occupied by $F(ab')_2$ fragments. (D) Addition of 100 nM BSA followed by several concentrations of TSH.

Even in buffer, a relatively high degree of undesired nonspecific binding (20−30%) has been measured,[28] suggesting that additional passivation steps are necessary. Finally, only nanomaterial-based sensors with relatively complex fabrication processes have been used which may limit the applications as a single-use disposable chip in a point-of-care environment.

In this work, we report a novel surface chemistry approach that combines antibody fragments as short biological receptors with polyethylene glycol (PEG) molecules to enable direct label-free selective immunodetection in whole serum with sub-pM detection limits—over 5 orders of magnitude lower than reported previously in buffer.[28] Thyroid-stimulating hormone (TSH) is chosen here as a representative analyte—a relevant and well-characterized immunosensing parameter with demanding sensitivity requirements. We demonstrate this approach with an extended-gate configuration, consisting of a gold sensing surface which is electrically connected to a commercial MOSFET transducer.[29] In previous work, various configurations of extended-gate FETs have been developed for biosensing applications, including silicon-based devices[30−32] and printed organic FETs.[27,33−35] A key advantage of the extended-gate approach over conventional electrolyte-gated layout is that the transducer is not in direct contact with the biological solution, avoiding possible reliability issues. Here, the transducer is also separated from the sensor chip. This allows reuse of the readout MOSFET, while the sensing chips can be independently designed as low-cost disposables with fewer fabrication steps compared to nanomaterial-based sensors.[36−38] The use of a gold surface gives access to well-established thiol-gold chemistry for self-assembled monolayers (SAMs) of linker molecules.[27,38−41] To evaluate the effect of PEG coimmobilization on the sensor response, two different surface modifications are compared, in the following referred to as "Mono SAM" and "Mix SAM". The Mono SAM only contains a short bifunctional PEG-based linker (SH-PEG-COOH, 0.5 kDa) to covalently attach the receptors and to prevent the denaturation of the proteins on gold,[42] while the Mix SAM additionally comprises a longer monofunctional PEG chain (SH-PEG, 10 kDa).

EXPERIMENTAL SECTION

Biomolecules. $F(ab')_2$ fragments of an anti-TSH antibody and the recombinant TSH antigen were kindly provided by Roche Diagnostics GmbH, Penzberg, Germany.

Sensor Modification. Prior to the modification, the gold was cleaned in base piranha (H_2O_2 (30%) + 1 part NH_4OH + 5 parts deionized (DI) water) for 15 min at 70 °C. After this, the gold was rinsed with DI water and dried with N_2. Just before the modification the gold was treated with oxygen plasma for 10 min. Every step of the modification protocol was performed using 50 mM MES buffer (pH 7). The first step was to incubate the gold for 5 min in buffer. Depending on the desired surface modification, the gold was incubated either in a solution of SH-PEG-COOH (0.5 kDa, 40 μM (celares) (for Mono SAM)) or in a 2 μM to 40 μM ratio of SH-PEG (10 kDa, nanocs) and 0.5 kDa SH-PEG-COOH (for Mix SAM) for 60 min. The sensor was then rinsed in buffer for 10 min to remove excess unbound PEG. The activation of the carboxyl groups on the surface was achieved by incubating the sensor for 20 min in a solution of *N*-ethyl-*N*′-(3-(dimethylamino)propyl) carbodiimide (EDC)/*N*-hydroxysuccinimide (NHS) from Sigma-Aldrich (0.4 mg/mL/0.6 mg/mL) for 20 min. Once the surface was activated, the sensors were incubated in a solution of anti-TSH $F(ab')_2$ antibody fragments (100 μg/mL at pH 5.6) for 60 min to immobilize the fragments via amino coupling reaction. This reaction is not site-specific and results in a random orientation of the receptors on the sensor surface. Excess $F(ab')_2$ fragments were removed by rinsing in buffer for 10 min. To prevent nonspecific binding on the surface the remaining binding sites on the surface (not covered by the $F(ab')_2$ fragments) were blocked by incubating the sensors in a 10 mg/mL bovine serum albumin (BSA) (Carl Roth) solution for 10 min.

QCM Measurements. The formation of both constructions used in this work (Mix and Mono SAM) on gold-coated quartz crystal was characterized using a Q-sense E4 from Biolin Scientific AB (Stockholm, Sweden) with an electrochemistry module. The mass deposited on the surface was recalculated from measured frequency changes using Q-tools software (Sauerbrey equation).

DOI: 10.1021/acssensors.7b00187
ACS Sens. 2017, 2, 1278−1286

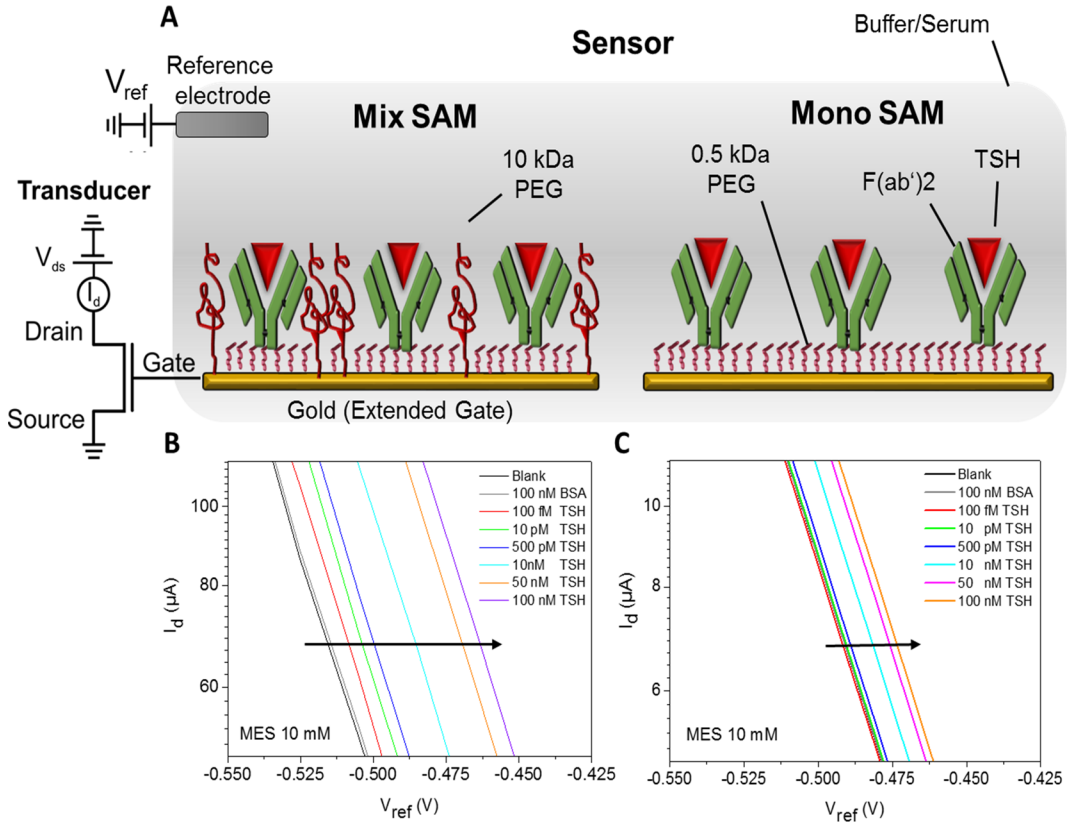

Figure 2. (A) Schematic representation of the sensor readout configuration, and both electrode types used to study the effect of PEG on the sensor response. Two different constructions were used: Mix SAM, consisting of a gold electrode modified with a self-assembled monolayer (SAM) of 0.5 kDa PEG, 10 kDa PEG, and F(ab′)$_2$ fragments; and Mono SAM consisting of a gold electrode modified with SAM based on 0.5 kDa PEG and F(ab′)$_2$ fragments. (B) Response of the sensor modified with the Mix SAM configuration to BSA and different concentrations of TSH in MES (10 mM, pH 7). (C) Response of the sensor modified with the Mono SAM configuration to BSA and different concentrations of TSH in MES (10 mM, pH 7).

Fabrication of Extended-Gate Electrodes. The electrodes were fabricated by thermal evaporation of Ti (10 nm) and Au (90 nm) onto glass slides (Borofloat 33, Schott) through a shadow mask. Each glass slide has 4 electrodes with the following lateral dimensions exposed to the fluid sample: 1.5 mm × 0.75 mm. The evaporation was performed at InnovationLab GmbH, Heidelberg.

Extended-Gate FET Measurements in Buffer and Serum. The sensor readout is shown in Figure 2A. The modified gold electrode was connected to the gate terminal of a commercial MOSFET from Microchip Technology (so-called extended gate configuration). A homemade silicone elastomer (Sylgard 184, Dow Corning) flow cell with PTFE inlet and outlet tubes (VWR) was assembled on top of the sensor chip. An Ag/AgCl reference electrode (World Precision Instruments, Dri-REF) was placed near the sensor surface inside the flow cell. A programmable syringe pump was used in withdrawal mode to deliver the samples to the sensor (Aladdin AL4000−220Z, World Precision Instruments). A constant flow rate of 40 μL/min was maintained during the experiments.

Electrical measurements were performed using a dual-channel source meter (Keithley 2636 B). Transfer curves were recorded by sweeping the potential applied to the reference electrode (V_{ref}) from −0.2 to −0.8 V. At the same time, a constant potential was applied between drain and source (V_{ds} = 0.1 V) and the drain-source current I_{ds} was monitored. The initial measurements were performed using different concentrations of human Thyroid Stimulating Hormone (TSH) or, as a control, 100 nM bovine serum albumin (BSA) in different concentrations of MES buffer at pH 7 (10 and 150 mM). After these tests, undiluted horse serum (Sigma-Aldrich) was spiked with different TSH concentrations and the measurements repeated. All sweep measurements were performed after 20 min of incubation with the required solution.

For real time binding experiments, a transfer curve (i.e., an I_{ds} vs V_{ref} sweep) was measured first to select a potential at an intermediate value of I_{sd} (around −0.4 V). Then, this constant potential was applied to the reference electrode (V_{ref}) while I_{ds} was monitored vs time at a constant V_{ds} = 0.1 V. To compare the real-time current changes to ΔV values obtained from sweeps, I_{ds} was then converted to voltage changes using the slope of the transfer curve (slope = $\Delta I_d/\Delta V_{ref}$) measured before the real-time measurement.

RESULTS AND DISCUSSION

Quartz Crystal Microbalance Study. As a first step, the surface modification protocol was established using a Quartz Crystal Microbalance (QCM). QCM is a mass-sensitive technique that relies on frequency changes of an oscillating quartz crystal upon adsorption of molecules on the surface. The QCM crystals used here were also coated with a gold film allowing a direct transfer of the successful functionalization protocol to the gold electrodes for electrical measurements. In Figure 1A, the main surface modification steps are schematically drawn for the Mix SAM surface, while the corresponding QCM measurements are presented in Figure 1B−D. This protocol consists of the following main steps: PEG SAM formation on gold, activation of the linker molecule (0.5 kDa SH-PEG-COOH) carbonyl groups present on the SAM with EDC/NHS (Figure 1B), followed by F(ab′)$_2$ fragment immobilization and blocking with bovine serum albumin (BSA), a commonly used and inexpensive blocking reagent (Figure 1C). It is clear from Figure 1 that the functionalization was successful because the

DOI: 10.1021/acssensors.7b00187
ACS Sens. 2017, 2, 1278−1286

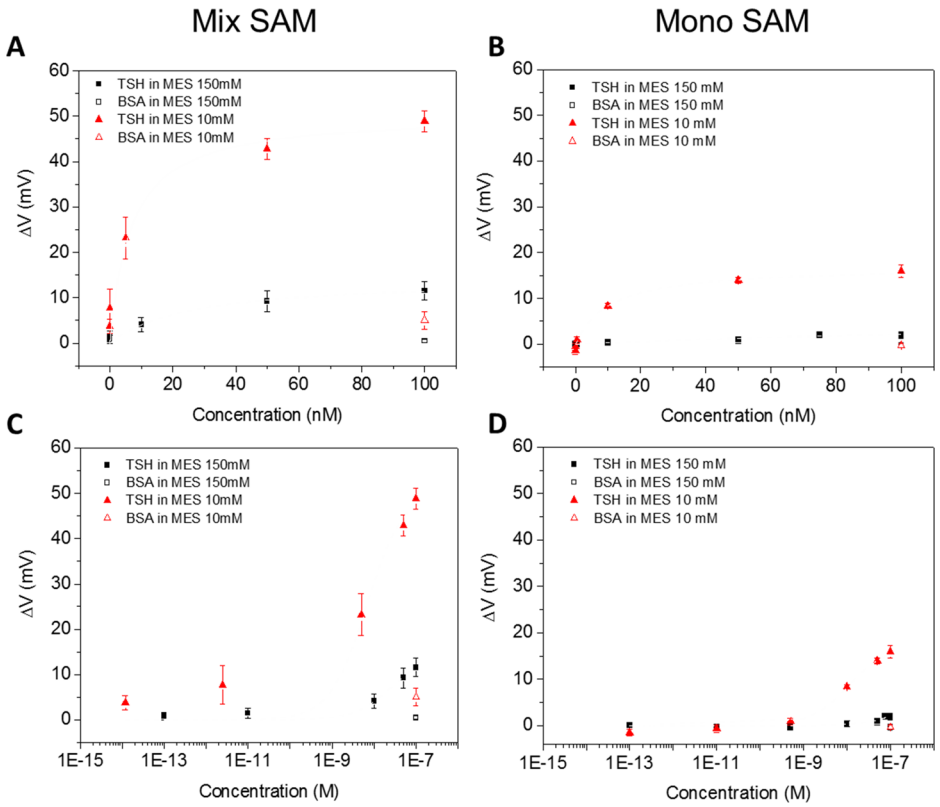

Figure 3. Plot of the potential change ΔV as a function of concentrations of TSH (filled symbols) and BSA (open symbols) in MES 10 mM (triangles) and in 150 mM (squares) in linear (A,B) and in semilogarithmic scale (C,D) for two different configurations: Mix SAM (A,C) and Mono SAM (B,C). Error bars correspond to the standard deviation from four experiments.

QCM oscillation frequency was lowered appreciably upon addition of Mix SAM (by approximately 16 Hz, Figure 1B), and further reduced by covalent binding of randomly oriented fragments (by approximately 15 Hz). This shift corresponds to a deposition of 387 ng/cm^2 (according to the Sauerbrey equation), similar to the values reported previously for this kind of antibodies (220−470 ng/cm^2).[43]

This immobilization is stable, as shown in Figure 1C from minute 160 to 190, where the frequency remains stable during 30 min under the flow of MES (50 mM, pH 7) indicating that the immobilized molecules remain on the surface and cannot be easily washed off. After that, the surface was incubated in 10 μM BSA solution to block the remaining active carbonyl groups that were not occupied by the antibody receptors (Figure 1C, starting at 195 min). Finally, the system was rinsed with buffer to wash off any loosely bound molecules.

After this buffer washing step, the functionality of this modification is demonstrated in Figure 1D by initially testing the nonspecific binding. For this purpose, we again choose BSA as a readily available protein that is frequently used to study nonspecific binding.[27] The sensor was exposed to a high concentration of BSA (100 nM), which did not change the QCM signal. Subsequently, several TSH concentrations were added ranging from 30 fM to 264 nM. No response to 30 fM of TSH is observed while a small change is visible upon addition of 30 pM TSH. A strong signal change of 9 Hz occurred with 30 nM TSH, followed by an additional decrease with 264 nM TSH. These results clearly indicate a successful and selective binding of TSH to the immobilized receptors. Similar results were obtained for the Mono SAM configuration (Figure S1).

Extended-Gate FET Measurements. Once the surface chemistry has been studied with QCM, we proceed with measurements of different TSH concentrations using the extended-gate readout shown in Figure 2A (more details are provided in the Experimental Section). The representative transfer curves obtained with both surfaces in 10 mM buffer are presented in Figure 2B,C. In both cases, the modified sensors could stabilize in buffer before the experiment, resulting in a stable baseline (blank). Then, the nonspecific binding was tested by exposing the sensor to 100 nM BSA, which is equimolar to the highest TSH concentration studied here. The BSA binding barely influenced the transfer curves, suggesting that the level of nonspecific binding is negligible, in agreement with QCM results. In contrast, a significant concentration-dependent response to TSH was observed, with the Mix SAM responding more strongly than Mono SAM, as indicated by arrows in Figure 2B,C (full transfer curves and enlarged views are shown in Figure S2). These results suggest that the coimmobilization of the 10 kDa polymer PEG indeed improves the sensor performance in 10 mM buffer.

However, it is still an open question whether this effect is sufficient to achieve a significant sensor response also in physiological ion concentration range (100−200 mM). To address this point, these experiments were repeated in 150 mM buffer, which falls into the relevant range. The results are compared in Figure 3. The measurements performed with the Mix SAM configuration (Figure 3A,C) show that, when a concentration of 10 mM MES buffer is used, the maximal signal obtained is around 4 times higher (51 mV at 100 nM TSH) than when 150 mM MES is used as a reading buffer (15 mV). Also, the limit of detection is different; it can be as low as 100

DOI: 10.1021/acssensors.7b00187
ACS Sens. 2017, 2, 1278−1286

fM TSH in 10 mM MES, while the LoD in 150 mM is around 3 orders of magnitude higher (~100 pM).

In the case of the Mono SAM construction, a similar dependence on ion concentration was found (Figure 3B,D). When 10 mM MES was used as reading buffer the maximal signal was higher (17 mV) compared to 150 mM MES buffer (<4 mV). Comparing the results obtained with both surface modifications we found that the Mix SAM is more sensitive to TSH than the Mono SAM construction in both 10 mM and 150 mM buffer. In fact, there was hardly any response in 150 mM buffer with the Mono SAM, whereas a clear TSH detection was demonstrated with the Mix SAM even in 150 mM solution.

Nonspecific binding of species other than the analyte also needs to be considered when designing a selective sensor. In all cases shown in Figure 3, the nonspecific signal obtained with 100 nM BSA is insignificant compared to the signal measured with the same concentration of TSH, clearly demonstrating the selectivity of the presented sensor for TSH. The low signal obtained with BSA can be attributed to the presence of the hydrophilic PEG on the surface.[27,44]

While the signal increase with decreasing ionic strength is expected since the Debye screening is reduced with fewer ions present in solution, the observed ~3× signal enhancement for the Mix SAM vs the Mono SAM at a given ionic strength is striking, because it enables direct analyte detection even in high ionic strength solutions such as the 150 mM buffer used here. Gao et al.[18] mentioned that the addition of PEG can change the dielectric properties of the interface. However, future work will be needed to provide a deeper quantitative understanding of this PEG-induced signal enhancement.

Motivated by these results (detection in high ionic strength and low nonspecific binding) obtained with the Mix SAM configuration, we decided to perform the same experiment using undiluted horse serum instead of buffer (Figure 4). Horse serum was chosen because it does not contain human TSH which would influence the calibration curve.

As seen in Figure 4 (black squares), the result of the experiment performed in serum at 21 °C (as all the previous experiments) using the Mix SAM configuration was very similar to the results achieved with the Mix SAM in 150 mM buffer (Figure 3A,C, squares). Despite the evident sensor response to TSH in horse serum at 21 °C, the limit of detection is in the nanomolar range (Figure 4B), far away from the usual TSH concentrations found in human serum (2–20 pM).[45] To further improve the sensor response and the LOD of the sensor in serum, we performed the experiment at 37 °C, because of expected faster association rate for this antibody–antigen interaction (according to manufacturer's data, the association rate should approximately double over this temperature range). The result of this experiment (Figure 4, squares) was a pronounced increase of the maximum sensor response by a factor of ~2 at very high TSH concentrations around 100 nM (Figure 4A) and a factor of ~3.5 in the low nM range (Figure 4B). Also, the entire curve at 37 °C is shifted toward lower TSH concentrations, which results in a lower detection limit as will be discussed later. The TSH concentration dependence is very robust and reproducible as the measurements were obtained with at least 3 devices per concentration (error bars represent the device-to-device variation), and repeated several weeks later with a new set of devices (downward triangles). In addition, real-time binding experiments were conducted for several low TSH concentrations (Figure S3). From this data, the signal after 20 min incubation was extracted and plotted as

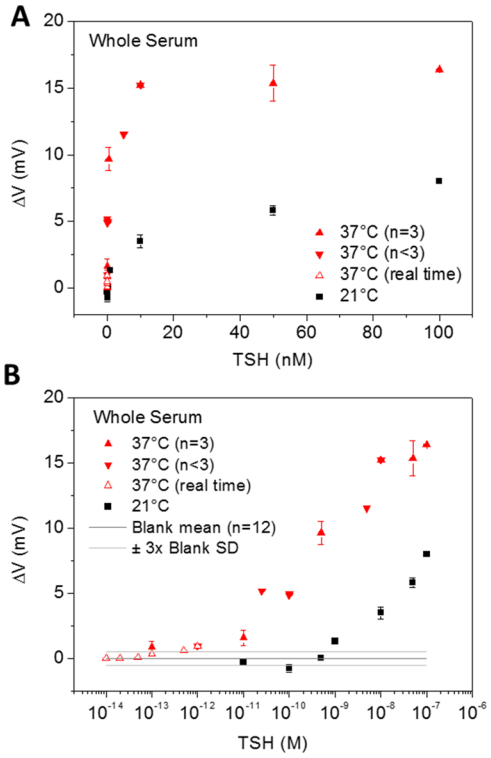

Figure 4. Results obtained with sensors modified with the Mix SAM configuration in horse serum spiked with different TSH concentrations, measured at 21 °C (squares) and at 37 °C (triangles). The same data is shown on linear (A) and semilogarithmic (B) scales. The horizontal lines in B represent the baseline fluctuations (mean value and ±3× SD).

open symbols in Figure 4B for comparison with the data from the transfer curves (that were also measured after 20 min incubation time). The maximum sensor response to 100 nM TSH and the lower detection limits for all experimental conditions used in this work are summarized in Table 1. Here,

Table 1. Summary of the Results Obtained in This Work[a]

temperature	sample	surface	ΔV_{max} (mV)	lower detection limit (M)
21 °C	MES 10 mM	Mono SAM	17	$<5 \times 10^{-10}$
21 °C	MES 10 mM	Mix SAM	51	$<1 \times 10^{-13}$
21 °C	MES 150 mM	Mono SAM	<4	–
21 °C	MES 150 mM	Mix SAM	12	$<1 \times 10^{-11}$
21 °C	Serum	Mix SAM	8	$<1 \times 10^{-09}$
37 °C	Serum	Mix SAM	17	5×10^{-13}

[a]Summary of the maximal signal obtained at 100 nM TSH (ΔV_{max}) and the lowest TSH concentration experimentally measured (lower limit of detection, LoD) for all conditions studied in this work.

the lower limit of detection is defined conventionally as LoD = $\Delta V_B + 3SD_B$ where ΔV_B is the mean signal obtained in blank serum samples without TSH, and SD_B is the corresponding standard deviation. To calculate the ΔV_B, a total of 12 different chips were measured in 4 different serum batches (3 chips per serum batch). This data is provided in the SI (Figure S4) and the resulting values are plotted as horizontal lines in Figure 4B: $\Delta V_B = 1.75 \times 10^{-5}$ V, $SD_B = 1.85 \times 10^{-4}$ V, and 3 $SD_B \sim 0.55$

DOI: 10.1021/acssensors.7b00187
ACS Sens. 2017, 2, 1278–1286

Table 2. Comparison of the TSH Detection Limits

technique	label	lower detection limit (pM)[c]	upper detection limit (pM)[c]	sample	total assay time	reference
Commercial ELISA	Yes	9.27	162	Buffer	>75 min	53
Time resolved fluorometry	Yes	0.16	464	Diluted Mouse Serum	>45 min	54
Electrochemiluminescence	Yes	5.80	580	Buffer	>60 min	55
Chemiluminescence	Yes	0.06	232	Serum	>65 min	56
Chemiluminescence-ELISA	Yes	11.01	319	Buffer	30 min	53
Scanning Force Microscopy	Yes	0.43	-	Buffer	>60 min	57
Electrochemistry	No	8.11	101	Buffer	>60 min	58
Silicon Nanowire FET	No	0.12	174	1 mM Buffer	<15 min	19
Commercial Electrochemiluminescence	Yes	0.03	580	Blood, Plasma, Serum[b]	18 min	[a]
Surface plasmon resonance	No	129	12000	Serum	20 min	59
Gold Extended Gate FET	No	0.5	10000	Serum	<20 min	This work

[a]Data obtained from FactSheet of Elecsys TSH (http://www.roche-diagnostics.ch/content/dam/corporate/roche-dia_ch/documents/broschueren/professional_diagnostics/serumarbeitsplatz/immunologie/schilddruesendiagnostik1/EN_TSH_FactSheet.pdf (retrieved on 10/02/2017). [b]Measurement performed in buffer after several incubation steps. [c]Some values were reported in μIU/mL. These results were converted to pM using the conversion factor for TSH of 1 μIU/mL = 5.6 pM according to World Health Organization (WHO)[60] (molecular weight of TSH ∼ 30 kDa).

mV. At 21 °C, only TSH concentrations above 1 nM can be reliably distinguished from the baseline fluctuations after 20 min of incubation. In contrast, all TSH concentrations ≥500 fM generate signals greater than 3× SD_B, when measured at 37 °C, indicating that the LoD is ∼500 fM for the same incubation time (20 min).

To better understand this strong effect of temperature, we performed a real-time measurement to compare the binding kinetics of TSH at 21 and 37 °C (Figure S5). This experiment demonstrates that TSH-induced signal grows faster at 37 °C compared to 21 °C, suggesting a faster association rate at elevated temperature. The slope of the signal change vs time rises by a factor of ∼1.84 from 21 to 37 °C, which agrees well with SPR data provided by the manufacturer for these specific antibodies (the association rate increases by a factor of ∼1.82 in this temperature range). Also, the experiment indicates that equilibrium may not be reached after 20 min (incubation time in all the experiments) at 21 °C, especially for low TSH concentrations <100 pM. Importantly, if we compare the signals in Figure S5 after 20 min of incubation, the response increases by approximately 3.5× if the temperature is raised from 21 to 37 °C. This enhancement is comparable to the signal increase measured after 20 min incubation in a similar TSH concentration range (Figure 4), indicating that both types of experiments yield consistent results when compared after the same incubation time. Similar improvement of the maximum response to TSH with increasing temperature was reported previously for other anti-TSH antibodies and detection methods,[46,47] and was also mainly attributed to improved binding of TSH to the receptor at higher temperature (i.e., faster reaction rate). We therefore conclude that a faster association rate at 37 °C for this particular antibody−antigen interaction can—at least partially—explain the observed signal enhancement. Other effects such as the temperature-dependent solubility and conformational changes of PEG[48,49] as well as faster diffusion of TSH to the sensor surface may also play a role and will motivate a more detailed study.

It is also important to realize that the results presented in Figure 4, measured after 20 min incubation time, are not necessarily in equilibrium, as supported by the real-time measurements shown in the SI. In general, the signal saturation time for an antigen−antibody interaction is strongly influenced by several factors such as the association rate, the dissociation rate (both quantities are temperature-dependent in this case), as well as the analyte concentration, and can easily exceed 20 min for high affinity antibodies at low analyte concentrations and low temperatures, as has been demonstrated earlier.[50] This means that the (equilibrium) dissociation constant K_d should not be estimated using this data. Based on the SPR data provided by the manufacturer, the expected K_d for this antibody−TSH interaction is <0.2 nM at 21 °C and 0.5 nM at 37 °C. The clear horizontal shift of the 21 °C curve toward higher analyte concentrations can be misinterpreted as a strong change of K_d. In fact, if such an estimate was attempted, the K_d (i.e., the TSH concentration at the half-maximum signal) would be strongly overestimated at 21 °C (>10 nM). The estimate at 37 °C (∼0.3 nM) agrees much better with the expected result, meaning that the signal at 37 °C is closer to equilibrium than the results at 21 °C, as expected.[50] Nevertheless, while faster kinetics at 37 °C can at least in part account for these differences, we cannot exclude at this point that other factors, such as the addition of PEG or the analyte diffusion, can also influence the binding of the analyte to the receptor.

From a practical point of view, if low concentrations of TSH are to be detected within 20 min, the assay should be performed at higher temperatures to generate more signal within the short available test time. On the other hand, the fundamental detection limit will depend on the type of the transducer used, and, in electronic devices, will be typically determined by the low-frequency noise.[51,52]

To the best of our knowledge, this is the first demonstration of direct immunodetection in undiluted serum using transistor-based biosensors. The majority of previous studies used reading buffers with a well-controlled low ionic strength to avoid the Debye screening,[2] sometimes in combination with signal enhancing labels. However, having a direct detection scheme offers many advantages such as simple workflow, reduced number of reagents and the liquid handling complexity—critical factors for the development of compact diagnostics devices with inexpensive disposable chips. Compared to previously mentioned aptamer-based direct detection approach by Gao et al.[28] (300 nM lower detection limit in 150 mM buffer), the presented method has 5 orders of magnitude lower detection limit and significantly lower nonspecific binding.

Importantly, among the existing TSH sensors (Table 2), the presented approach is the only direct method that does not

DOI: 10.1021/acssensors.7b00187
ACS Sens. 2017, 2, 1278−1286

require any labels or washing steps, and can potentially be operated in an inexpensive hand-held point-of-care instrument. Compared to the state-of-the-art TSH detection, currently performed on central laboratory analyzers via an elaborate electrochemiluminescence sandwich immunoassay, the present direct approach shows a higher lower detection limit and a much higher upper detection limit in serum (Table 2). The presented measurement range (~0.5−10 000 pM) already covers the physiological TSH concentration (2−20 pM) and may be further improved in future optimization studies. As well, more work is still needed to assess the performance of the sensor in whole blood, and to determine the accuracy vs the state of the art. Finally, it should be noted that this approach is not limited to TSH and can also be applied to other analytes with different sensitivity requirements.

CONCLUSIONS

In conclusion, direct, label-free and specific immunodetection of thyroid-stimulating hormone in whole serum was demonstrated. Extended-gate field-effect transistors with a gold sensing surface were used as simple and robust electronic transducers. To overcome the Debye screening, a mixed functionalization layer was developed consisting of short biological receptors (antibody fragments) and a polyethylene glycol layer (PEG). With this mixed surface, a 3-fold signal enhancement was achieved compared to the control surface without the PEG molecules. In addition, the lower detection limit could be dramatically improved below 500 fM if the measurements were carried out in serum at 37 °C instead of 21 °C. Under these conditions, the sensor offers a competitive performance compared to state-of-the-art technology, and can be further improved in the future. The presented approach is universal, fast (<20 min), and low cost, does not require any washing steps or sample pretreatment, and can enable the next generation of point-of-care diagnostics devices with performance of central laboratory analyzers.

ASSOCIATED CONTENT

Supporting Information

The Supporting Information is available free of charge on the ACS Publications website at DOI: 10.1021/acssensors.7b00187.

QCM data for Mono SAM configuration; detailed data from Figure 2; measurements in blank serum; real-time measurements in serum; real-time measurements at different temperatures (PDF)

AUTHOR INFORMATION

Corresponding Author

*E-mail: tarasov@bio.mx.

ORCID

Óscar Gutiérrez-Sanz: 0000-0001-7559-9204
Nesha M. Andoy: 0000-0002-5326-3328
Marcin S. Filipiak: 0000-0002-7649-4890
Alexey Tarasov: 0000-0003-2811-5988

Notes

The authors declare no competing financial interest.

ACKNOWLEDGMENTS

The research of the team "Nanomaterial-Based Biosensors" at BioMed X Innovation Center is kindly sponsored by Roche Diagnostics GmbH. The authors thank Dr. Pavel Kubalec and Dr. Tobias Oelschlaegel (Roche Diagnostics GmbH) for providing $F(ab')_2$ fragments of an anti-TSH antibody, recombinant TSH antigen, and for fruitful discussions. The authors are grateful to Dr. Michael Hein (Roche Diagnostics International Ltd.), Dr. Dieter Heindl, Dr. Moritz Marcinowski, Dr. Heiko Mussauer, Dr. Reiner Schlipfenbacher, Dr. Jürgen Spinke (Roche Diagnostics GmbH), and Prof. Dr. Jana Zaumseil (Universität Heidelberg) for numerous valuable discussions. The authors thank Dr. Arnulf Staib (Roche Diabetes Care GmbH) for providing access to the quartz crystal microbalance. The authors also thank Anton Malovichko for assistance with the design of the measurement setup.

REFERENCES

(1) Noor, M. O.; Krull, U. J. Silicon nanowires as field-effect transducers for biosensor development: A review. *Anal. Chim. Acta* **2014**, *825* (0), 1−25.

(2) Mu, L.; Chang, Y.; Sawtelle, S. D.; Wipf, M.; Duan, X.; Reed, M. Silicon nanowire field-effect transistors—A versatile class of potentiometric nanobiosensors. *IEEE Access* **2015**, *3*, 287−302.

(3) Zhang, A.; Lieber, C. M. Nano-bioelectronics. *Chem. Rev.* **2016**, *116* (1), 215−257.

(4) Chamorro-Garcia, A.; Merkoçi, A. Nanobiosensors in diagnostics. *Nanobiomedicine* **2016**, *3*, 1−26.

(5) Star, A.; Tu, E.; Niemann, J.; Gabriel, J.-C. P.; Joiner, C. S.; Valcke, C. Label-free detection of DNA hybridization using carbon nanotube network field-effect transistors. *Proc. Natl. Acad. Sci. U. S. A.* **2006**, *103* (4), 921−926.

(6) Kharitonov, A. B.; Zayats, M.; Lichtenstein, A.; Katz, E.; Willner, I. Enzyme monolayer-functionalized field-effect transistors for biosensor applications. *Sens. Actuators, B* **2000**, *70* (1−3), 222−231.

(7) Bergveld, P. Development of an Ion-Sensitive Solid-State Device for Neurophysiological Measurements. *IEEE Trans. Biomed. Eng.* **1970**, *BME-17* (1), 70−71.

(8) Caras, S.; Janata, J. Field effect transistor sensitive to penicillin. *Anal. Chem.* **1980**, *52* (12), 1935−1937.

(9) Bergveld, P. Thirty years of ISFETOLOGY: What happened in the past 30 years and what may happen in the next 30 years. *Sens. Actuators, B* **2003**, *88* (1), 1−20.

(10) Cui, Y.; Wei, Q.; Park, H.; Lieber, C. M. Nanowire nanosensors for highly Sensitive and Selective detection of biological and chemical species. *Science* **2001**, *293* (5533), 1289−1292.

(11) Knopfmacher, O.; Tarasov, A.; Fu, W.; Wipf, M.; Niesen, B.; Calame, M.; Schönenberger, C. Nernst limit in dual-gated Si-nanowire FET sensors. *Nano Lett.* **2010**, *10* (6), 2268−2274.

(12) Tarasov, A.; Wipf, M.; Stoop, R. L.; Bedner, K.; Fu, W.; Guzenko, V. A.; Knopfmacher, O.; Calame, M.; Schönenberger, C. Understanding the electrolyte background for biochemical sensing with ion-sensitive field-effect transistors. *ACS Nano* **2012**, *6* (10), 9291−9298.

(13) Wipf, M.; Stoop, R. L.; Tarasov, A.; Bedner, K.; Fu, W.; Wright, I. A.; Martin, C. J.; Constable, E. C.; Calame, M.; Schönenberger, C. Selective sodium sensing with gold-coated silicon nanowire field-effect transistors in a differential setup. *ACS Nano* **2013**, *7* (7), 5978−5983.

(14) Stern, E.; Klemic, J. F.; Routenberg, D. A.; Wyrembak, P. N.; Turner-Evans, D. B.; Hamilton, A. D.; LaVan, D. A.; Fahmy, T. M.; Reed, M. A. Label-free immunodetection with CMOS-compatible semiconducting nanowires. *Nature* **2007**, *445* (7127), 519−522.

(15) https://www.thermofisher.com/de/de/home/life-science/sequencing/next-generation-sequencing/ion-torrent-next-generation-sequencing-workflow/ion-torrent-next-generation-sequencing-select-targets/ampliseq-target-selection.html (retrieved on 10/02/2017).

(16) http://www.vistatherapeutics.org/ (retrieved on 10/02/2017).

(17) Turner, A. P. F. Biosensors: sense and sensibility. *Chem. Soc. Rev.* **2013**, *42* (8), 3184−3196.

DOI: 10.1021/acssensors.7b00187
ACS Sens. 2017, 2, 1278−1286

(18) Shoorideh, K.; Chui, C. O. On the origin of enhanced sensitivity in nanoscale FET-based biosensors. *Proc. Natl. Acad. Sci. U. S. A.* **2014**, *111* (14), 5111−5116.
(19) Lu, N.; Dai, P.; Gao, A.; Valiaho, J.; Kallio, P.; Wang, Y.; Li, T. Label-free and rapid electrical detection of hTSH with CMOS-compatible silicon nanowire transistor arrays. *ACS Appl. Mater. Interfaces* **2014**, *6* (22), 20378−20384.
(20) Gao, N.; Zhou, W.; Jiang, X.; Hong, G.; Fu, T.-M.; Lieber, C. M. General strategy for biodetection in high honic strength solutions using transistor-based nanoelectronic sensors. *Nano Lett.* **2015**, *15* (3), 2143−2148.
(21) Stern, E.; Wagner, R.; Sigworth, F. J.; Breaker, R.; Fahmy, T. M.; Reed, M. A. Importance of the debye screening length on nanowire field effect transistor sensors. *Nano Lett.* **2007**, *7* (11), 3405−3409.
(22) Vigneshvar, S.; Sudhakumari, C. C.; Senthilkumaran, B.; Prakash, H. Recent advances in biosensor technology for potential applications − An Overview. *Front. Bioeng. Biotechnol.* **2016**, *4*, 11.
(23) Israelachvili, J. N. *Intermolecular and surface forces*; Elsevier Science, 2011.
(24) Elnathan, R.; Kwiat, M.; Pevzner, A.; Engel, Y.; Burstein, L.; Khatchtourints, A.; Lichtenstein, A.; Kantaev, R.; Patolsky, F. Biorecognition layer engineering: overcoming screening limitations of nanowire-based FET devices. *Nano Lett.* **2012**, *12* (10), 5245−5254.
(25) Kulkarni, G. S.; Zhong, Z. Detection beyond the Debye screening length in a high-frequency nanoelectronic biosensor. *Nano Lett.* **2012**, *12* (2), 719−723.
(26) Cheng, S.; Hotani, K.; Hideshima, S.; Kuroiwa, S.; Nakanishi, T.; Hashimoto, M.; Mori, Y.; Osaka, T. Field Effect Transistor biosensor using antigen binding fragment for detecting tumor marker in human serum. *Materials* **2014**, *7* (4), 2490.
(27) White, S. P.; Sreevatsan, S.; Frisbie, C. D.; Dorfman, K. D. Rapid, selective, label-free aptameric capture and detection of ricin in potable liquids using a printed floating gate transistor. *ACS Sens.* **2016**, *1* (10), 1213−1216.
(28) Gao, N.; Gao, T.; Yang, X.; Dai, X.; Zhou, W.; Zhang, A.; Lieber, C. M. Specific detection of biomolecules in physiological solutions using graphene transistor biosensors. *Proc. Natl. Acad. Sci. U. S. A.* **2016**, *113* (51), 14633−14638.
(29) Tarasov, A.; Gray, D. W.; Tsai, M.-Y.; Shields, N.; Creedon, N.; Montrose, A.; Lovera, P.; O'Riordan, A.; Mooney, M. H.; Vogel, E. M. A potentiometric biosensor for rapid on-site disease diagnostics. *Biosens. Bioelectron.* **2016**, *79*, 669−678.
(30) Kim, D. S.; Park, J. E.; Shin, J. K.; Kim, P. K.; Lim, G.; Shoji, S. An extended gate FET-based biosensor integrated with a Si microfluidic channel for detection of protein complexes. *Sens. Actuators, B* **2006**, *117* (2), 488−494.
(31) Rothberg, J. M.; Hinz, W.; Rearick, T. M.; Schultz, J.; Mileski, W.; Davey, M.; Leamon, J. H.; Johnson, K.; Milgrew, M. J.; Edwards, M.; Hoon, J.; Simons, J. F.; Marran, D.; Myers, J. W.; Davidson, J. F.; Branting, A.; Nobile, J. R.; Puc, B. P.; Light, D.; Clark, T. A.; Huber, M.; Branciforte, J. T.; Stoner, I. B.; Cawley, S. E.; Lyons, M.; Fu, Y.; Homer, N.; Sedova, M.; Miao, X.; Reed, B.; Sabina, J.; Feierstein, E.; Schorn, M.; Alanjary, M.; Dimalanta, E.; Dressman, D.; Kasinskas, R.; Sokolsky, T.; Fidanza, J. A.; Namsaraev, E.; McKernan, K. J.; Williams, A.; Roth, G. T.; Bustillo, J. An integrated semiconductor device enabling non-optical genome sequencing. *Nature* **2011**, *475* (7356), 348−352.
(32) Guan, W.; Duan, X.; Reed, M. A. Highly specific and sensitive non-enzymatic determination of uric acid in serum and urine by extended gate field effect transistor sensors. *Biosens. Bioelectron.* **2014**, *51*, 225−231.
(33) Minami, T.; Sato, T.; Minamiki, T.; Tokito, S. An extended-gate type organic FET based biosensor for detecting biogenic amines in aqueous solution. *Anal. Sci.* **2015**, *31* (7), 721−724.
(34) Minamiki, T.; Minami, T.; Kurita, R.; Niwa, O.; Wakida, S.-i.; Fukuda, K.; Kumaki, D.; Tokito, S. Accurate and reproducible detection of proteins in water using an extended-gate type organic transistor biosensor. *Appl. Phys. Lett.* **2014**, *104* (24), 243703.
(35) White, S. P.; Dorfman, K. D.; Frisbie, C. D. Label-free DNA sensing platform with low-voltage electrolyte-gated transistors. *Anal. Chem.* **2015**, *87* (3), 1861−1866.
(36) Tiwari, J. N.; Vij, V.; Kemp, K. C.; Kim, K. S. Engineered carbon-nanomaterial-based electrochemical sensors for biomolecules. *ACS Nano* **2016**, *10* (1), 46−80.
(37) Liu, X.; Tao, H.; Yang, K.; Zhang, S.; Lee, S.-T.; Liu, Z. Optimization of surface chemistry on single-walled carbon nanotubes for in vivo photothermal ablation of tumors. *Biomaterials* **2011**, *32* (1), 144−151.
(38) Tarasov, A.; Tsai, M.-Y.; Flynn, E. M.; Joiner, C. A.; Taylor, R. C.; Vogel, E. M. Gold-coated graphene field-effect transistors for quantitative analysis of protein−antibody interactions. *2D Mater.* **2015**, *2* (4), 044008.
(39) Frasconi, M.; Mazzei, F.; Ferri, T. Protein immobilization at gold−thiol surfaces and potential for biosensing. *Anal. Bioanal. Chem.* **2010**, *398* (4), 1545−1564.
(40) Wouters, D.; Schubert, U. S. Nanolithography and nano-chemistry: probe-related patterning techniques and chemical modification for nanometer-sized devices. *Angew. Chem., Int. Ed.* **2004**, *43* (19), 2480−2495.
(41) Wipf, M.; Stoop, R. L.; Navarra, G.; Rabbani, S.; Ernst, B.; Bedner, K.; Schönenberger, C.; Calame, M. Label-Free FimH protein interaction analysis using silicon nanoribbon bioFETs. *ACS Sens.* **2016**, *1* (6), 781−788.
(42) Yoshimoto, K.; Nishio, M.; Sugasawa, H.; Nagasaki, Y. Direct observation of adsorption-induced inactivation of antibody fragments surrounded by mixed-PEG layer on a gold surface. *J. Am. Chem. Soc.* **2010**, *132* (23), 7982−7989.
(43) Bonroy, K.; Frederix, F.; Reekmans, G.; Dewolf, E.; De Palma, R.; Borghs, G.; Declerck, P.; Goddeeris, B. Comparison of random and oriented immobilisation of antibody fragments on mixed self-assembled monolayers. *J. Immunol. Methods* **2006**, *312* (1−2), 167−181.
(44) Rastogi, A.; Nad, S.; Tanaka, M.; Mota, N. D.; Tague, M.; Baird, B. A.; Abruña, H. D.; Ober, C. K. Preventing nonspecific adsorption on polymer brush bovered gold electrodes using a modified ATRP initiator. *Biomacromolecules* **2009**, *10* (10), 2750−2758.
(45) Garber, J.; Cobin, R.; Gharib, H.; Hennessey, J.; Klein, I.; Mechanick, J.; Pessah-Pollack, R.; Singer, P.; Woeber, K. Clinical practice guidelines for hypothyroidism in adults: cosponsored by the American association of clinical endocrinologists and the American thyroid association. *Endocr. Pract.* **2012**, *18* (6), 988−1028.
(46) Bashford, C. L.; Harrison, S. J.; Radda, G. K.; Mehdi, Q. The relation between lipid mobility and the specific hormone binding of thyroid membranes. *Biochem. J.* **1975**, *146* (2), 473−479.
(47) Schräml, M.; von Proff, L. Temperature-dependent antibody kinetics as a tool in antibody lead selection. *In Antibody Methods and Protocols*, Proetzel, G.; Ebersbach, H., Eds. Humana Press: Totowa, NJ, 2012; pp 183−194.
(48) Lee, J.; Joo, M. K.; Kim, J.; Park, J. S.; Yoon, M.-Y.; Jeong, B. Temperature-sensitive biodegradable poly(ethylene glycol). *J. Biomater. Sci., Polym. Ed.* **2009**, *20* (7−8), 957−965.
(49) Pasche, S.; Vörös, J.; Griesser, H. J.; Spencer, N. D.; Textor, M. effects of ionic strength and surface charge on protein adsorption at pegylated surfaces. *J. Phys. Chem. B* **2005**, *109* (37), 17545−17552.
(50) Andersson, K., et al. Antibody-antigen interactions: What is the required time to equilibrium? *Nature Precedings*, **2010**. DOI: 10101/npre.2010.5218.1.
(51) Tarasov, A.; Fu, W.; Knopfmacher, O.; Brunner, J.; Calame, M.; Schönenberger, C. Signal-to-noise ratio in dual-gated silicon nanoribbon field-effect sensors. *Appl. Phys. Lett.* **2011**, *98* (1), 012114−012114−3.
(52) Bedner, K.; Guzenko, V. A.; Tarasov, A.; Wipf, M.; Stoop, R. L.; Rigante, S.; Brunner, J.; Fu, W.; David, C.; Calame, M. Investigation of the dominant 1/f noise source in silicon nanowire sensors. *Sens. Actuators, B* **2014**, *191*, 270−275.
(53) Jung, W.; Han, J.; Kai, J.; Lim, J.-Y.; Sul, D.; Ahn, C. H. An innovative sample-to-answer polymer lab-on-a-chip with on-chip

DOI: 10.1021/acssensors.7b00187
ACS Sens. 2017, 2, 1278−1286

reservoirs for the POCT of thyroid stimulating hormone (TSH). *Lab Chip* **2013**, *13* (23), 4653−4662.
(54) Wu, F.-B.; Han, S.-Q.; Xu, T.; He, Y.-F. Sensitive time-resolved fluoroimmunoassay for simultaneous detection of serum thyroid-stimulating hormone and total thyroxin with Eu and Sm as labels. *Anal. Biochem.* **2003**, *314* (1), 87−96.
(55) Helin, M.; Väre, L.; Håkansson, M.; Canty, P.; Hedman, H. P.; Heikkilä, L.; Ala-Kleme, T.; Kankare, J.; Kulmala, S. Electrochemiluminoimmunoassay of hTSH at disposable oxide-coated n-silicon electrodes. *J. Electroanal. Chem.* **2002**, *524*−*525*, 176−183.
(56) Lin, Z.; Wang, X.; Li, Z.-J.; Ren, S.-Q.; Chen, G.-N.; Ying, X.-T.; Lin, J.-M. Development of a sensitive, rapid, biotin−streptavidin based chemiluminescent enzyme immunoassay for human thyroid stimulating hormone. *Talanta* **2008**, *75* (4), 965−972.
(57) Perrin, A.; Theretz, A.; Mandrand, B. Thyroid Stimulating Hormone Assays Based on the detection of gold conjugates by scanning force microscopy. *Anal. Biochem.* **1998**, *256* (2), 200−206.
(58) Lin, Z.-H.; Shen, G.-L.; Miao, Q.; Yu, R.-Q. A thyroid-stimulating hormone immuno-electrode. *Anal. Chim. Acta* **1996**, *325* (1), 87−92.
(59) Treviño, J.; Calle, A.; Rodríguez-Frade, J.m.; Mellado, M.; Lechuga, L. Surface plasmon resonance immunoassay analysis of pituitary hormones in urine and serum samples. *Clin. Chim. Acta* **2009**, *403* (1), 56−62.
(60) WHO International standard thyroid stimulating hormone, human, for immunoassay. NIBSC code 81/565 (Version 6.0, Dated 08/04/2015). https://www.thermofisher.com/de/de/home/life-science/sequencing/next-generation-sequencing/ion-torrent-next-generation-sequencing-workflow/ion-torrent-next-generation-sequencing-select-targets/ampliseq-target-selection.html (retrieved on 10/02/2017).

DOI: 10.1021/acssensors.7b00187
ACS Sens. 2017, 2, 1278−1286